ELSEVIER

Tectonophysics 266 (1996) 187–201

TECTONOPHYSICS

# Kinematic modelling of large-scale structural asymmetry across the Dead Sea Rift

S. Wdowinski [a,*], Ezra Zilberman [b]

[a] *Department of Geophysics and Planetary Sciences, Tel Aviv University, Ramat Aviv, 69978, Israel*
[b] *Geological Survey of Israel, 30 Malkhe Israel St., Jerusalem, 95501, Israel*

Received 20 June 1996; accepted 2 October 1996

**Abstract**

The Dead Sea Rift (DSR) is characterized by large-scale topographic and structural asymmetries: the rift's eastern side is flexed upward toward the axis and its overall shape resembles an uplifted shoulder; the western side of the rift is flexed down toward the axis and its overall shape resembles a wide arch. We use a kinematic model of the lithosphere to explain the cumulative deformation of the pre-rift topography in response to two tectonic processes: normal faulting due to lithospheric extension and isostatic uplift. The model considers the sum relief of three surfaces: relief that existed prior to the formation of the rift (initial topography), relief created by slip along a curved normal boundary fault (kinematic topography), and relief created by isostatic response of the lithosphere to this faulting and to an additional unmodelled load (isostatic topography). The model predicts the observed structure across the rift only when we considered a significant additional load, comparable in magnitude to the load induced by the kinematic topography. The additional load reflects the negative mass anomaly of the 8–10-km-deep Dead Sea Basin, which is filled with unconsolidated sediments. By constraining the model with the structural observations, we determined that the extension perpendicular to the rift axis lies in the range 1–4 km in the northern half of the rift and 2–8 km in the southern half. The model also explains other observations across the DSR, such as the configuration of the three present-day regional drainage systems and the observed low-magnitude upward deflection of the Moho beneath the rift.

*Keywords:* kinematic topography; kinematic modelling; Dead Sea Rift; crustal structure

## 1. Introduction

The Dead Sea Rift (DSR) is a long and narrow morphological depression that extends from the Gulf of Elat (Aqaba) 500 km northward to the Bakaa Valley (about 150 km north of Lake Kinneret) (Fig. 1a). It lies along the Dead Sea Transform (DST), which separates the Arabian plate from the Israel–Sinai sub-plate (inset Fig. 1a) (Wilson, 1965; Freund et al., 1970; Garfunkel, 1981). It is characterized by two sets of structures: (1) long and narrow (<20 km wide) pull-apart basins bounded by strike-slip faults and lying within the narrow rift valley; and (2) wide regional flexural structures (>50 km) bounded by normal faults along the rift valley, but extending well beyond the narrow rift valley (Fig. 2).

The formation of the DSR is generally examined in the context of the elongate structures within the rift, whose development is attributed to horizontal displacements along strike-slip faults arranged in an

* Corresponding author; E-mail shimon@geo1.tau.ac.il.


*PII* S0040-1951(96)00238-7

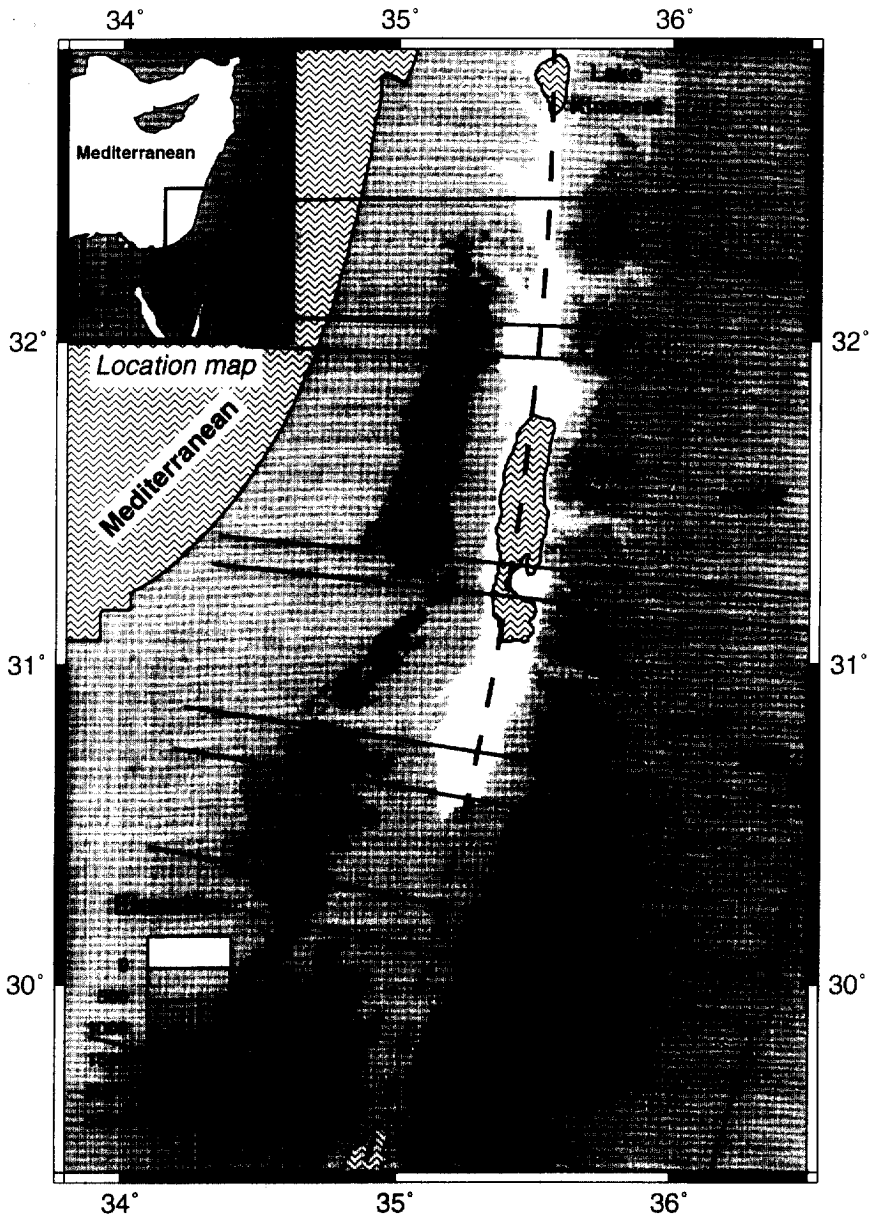


Fig. 1. (a) Shaded topographic map of the area surrounding the Dead Sea Rift between Lake Kinneret and the Red Sea. The dashed line shows the location of the small (latitudinal) circle that best describes the rift axis. The map also displays the locations of the five segments that show similar long-wavelength topography (see text and b). (b) Topographic (solid) and TES (dashed–dotted) profiles across the five segments of similar topography (a). The profiles represent the mean topography and the TES elevation in the profiles presented by Wdowinski and Zilberman (1996).

en-echelon pattern (Quenell, 1959; Freund et al., 1970; Garfunkel, 1981). Recently, Ben-Avraham and Zobak (1992) suggested that the asymmetry of the Dead Sea basin cannot be explained by a pull-apart basin model. They proposed an alternative model, in which the horizontal motion is accommodated by a single transform fault, and the extension by parallel normal faults. However, both the pull-apart basin and

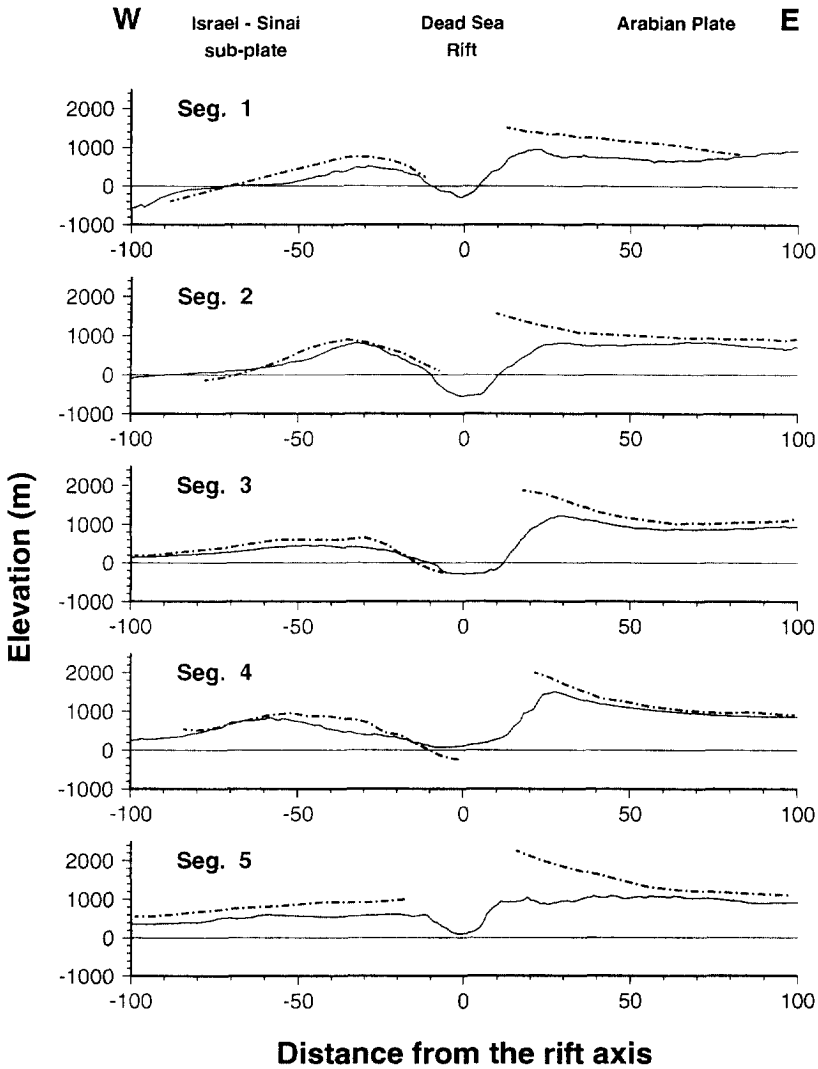


Fig. 1. Continued.

the alternative models are concerned with structures that lie within the narrow rift and ignore the larger regional-scale flexural structure. This structure is characterized by a distinct asymmetry (Fig. 2): the rift's eastern margin is flexed upward toward the axis and its overall shape resembles an uplifted shoulder, whereas the western margin is flexed down toward the axis and its overall shape resembles a wide arch (Wdowinski and Zilberman, 1996).

Similar large-scale asymmetries occur along the East African Rift (EAR), where they are very pronounced and have been extensively studied (e.g., Rosendahl, 1987; Ebinger et al., 1989). Ebinger et al. (1991) investigated the topography and free-air gravity anomalies across the East African Rift using an isostatically uplifted half-graben model based on the formulation of Weissel and Karner (1989). Ebinger et al. (1991) showed that both the topography and the gravity anomalies can be explained by a small amount of extension (3–10 km) perpendicular to the rift axis and by a significant flexural strength of the lithosphere maintained during the extension. A similar model was successfully applied by Bell et al. (1988) to explain the Bouguer gravity anoma-

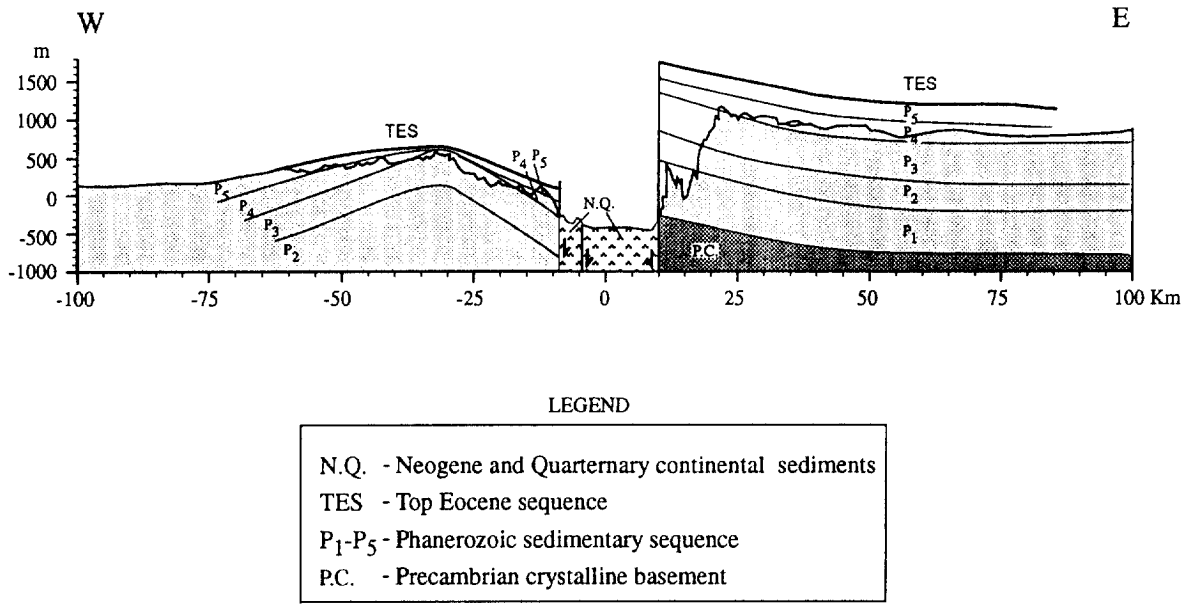


Fig. 2. Schematic geologic sections across the DSR showing the large-scale asymmetric structure across the rift. The section displays the major rock units and the reconstructed location of the TES marker perpendicular to the rift axis. The section is based on geological sections presented by Wdowinski and Zilberman (1996).

lies across the Newark and Gettysburg basins in the mid-Atlantic region off the North American east coast.

Although the DSR and the EAR have developed in very different tectonic environments, the first along a transform plate boundary and the latter within a plate interior, the similar large-scale asymmetry across the two rift systems may suggest a similar mechanism for the formation of the two rifts. This study aims to explain the large-scale asymmetry across the DSR by modelling it as an isostatically supported half-graben, similar to the model of Ebinger et al. (1991). Half-graben structures have previously been invoked to explain some strongly asymmetric segments of the rift (Picard, 1966, 1987). Isostatic uplift of the lithosphere along the rift's axis has also been proposed as a mechanism for the uplifted topography in the region (Ten Brink et al., 1990); however, Ten Brink et al. (1990) considered a single profile across the rift in a locality where the topography is nearly symmetric and therefore not representative. The present study considers the combined effect of half-graben structure development and isostatic uplift, taking into account the pre-rift morphology, to generate a quantitative model that successfully explains the observed large-scale asymmetry across DSR.

## 2. Observations

Geological and geophysical studies of the DSR provide essential observations to constrain quantitative models. Here we provide a brief summary of the key observations: large-scale topography, structure, morphology, and crustal structure across the rift. These observations are described extensively by Wdowinski and Zilberman (1996).

### *2.1. Tectonic background*

The DSR is one of the most pronounced expressions of a continental breakup process that influenced the region since the mid-Cenozoic. The present-day morphology of the DSR was formed in Early Pliocene (5–4 Ma) (Picard, 1951; Bentor and Vroman, 1960) along the trace of the DST. The left-lateral motion along the DST was initiated much earlier, in the Early Miocene (26 Ma), and has accumulated a total of 105 km (Freund et al., 1970; Garfunkel, 1981). The displacement along the DST

since the formation of the rift in the Pliocene is 30 km (Joffe and Garfunkel, 1987).

### 2.2. Topography

The large-scale topography along the DSR shows a distinct asymmetry across the rift axis (Fig. 1). The higher elevation occurs on the eastern side, where the overall shape resembles an uplifted shoulder; the western side resembles a wide arch. A systematic analysis of the large-scale topography, between Lake Kinneret and the Gulf of Elat, shows distinct along-strike variations (Wdowinski and Zilberman, 1996). Five segments have been distinguished based on differences in the shape and height of the eastern shoulder, and the amplitude and width of the arch (Fig. 1b). Two of the five segments portray a less pronounced asymmetry. In Segment 2, which lies along the deepest part of the rift (the northern basin of the Dead Sea), both sides are of a similar elevation, although the characteristic shape of each side is maintained. In Segment 5, which is located near the Gulf of Elat, both sides of the rift resemble uplifted shoulders; however, the sense of asymmetry remains because the highest elevation occurs on the eastern side.

### 2.3. Structure

The large-scale structure across the DSR was systematically analyzed along the same segments as the topography. The structure can be traced in considerable detail because the rift margins are built of a thick sequence of sedimentary rock units that provide excellent markers (Fig. 2). Although the observed structure reflects the cumulative deformation since the formation of these rock units, Wdowinski and Zilberman (1996) were able to separate the rift-related structure from the cumulative structure by identifying and using a regional marker: the Top Eocene Sequence (TES). This marker represents the roof of the Eocene rock unit, which was deposited during the last regional transgression, forming a continuous flat surface slightly inclined to the northwest. During the Oligocene, the TES experienced negligible deformation (Wdowinski and Zilberman, 1996). Thus, the observed vertical deflection of the TES represents the post-Oligocene rift-related deformation of the pre-rift topography.

The TES marker shows that the large-scale structure across the rift is also characterized by an asymmetric pattern similar to that of the topography (Figs. 1b and 2). The western side structure resembles a wide (60–100 km wide) asymmetric anticline, which Picard (1943) named 'arching'. The transition between the two structures lies within the narrow depression of the rift, which is filled by a thick sequence of continental sediments. As in the topography analysis, along strike variations of the large-scale structure are characterized by the shape and height of the eastern side uplifted margin and the amplitude and width of the western side arching. There is one exception, Segment 5, which has an uplifted western margin instead of the down flexed margin characteristic of the rest of the segments.

### 2.4. Morphology

The regional morphology follows a general N–S direction parallel to the DSR (Fig. 3). It is well expressed by the configuration of the regional drainage network, which consists of three systems: the Mediterranean, the DSR, and the Transjordan closed drainage basins. The DSR drainage system has two base levels, the Dead Sea (−400 m) and the Gulf of Elat (sea level), which are separated in the central Arava Valley at an elevation of 200 m. The Transjordan closed drainage basins (El Azaraq in the north and El Jafar in the south) lie 80–150 km east of the rift axis at an elevation of 700–900 m above sea level.

The present-day physiography, made up of three separate drainage systems, developed in the Early Pliocene (5–4 Ma) (Picard, 1951; Bentor and Vroman, 1960). During the Oligocene and most of the Miocene (38–5 Ma), the entire region was part of a single morphological unit that drained northwestward to the Mediterranean (Picard, 1951; Garfunkel and Horowitz, 1966). This pre-rift morphology was characterized by a low surface relief with a slight northwestward gradient (Zilberman, 1984, 1992).

### 2.5. Crustal structure

Gravity and seismic refraction studies have been used to detect the deeper structure of two markers across the rift: the upper surface of the crystalline

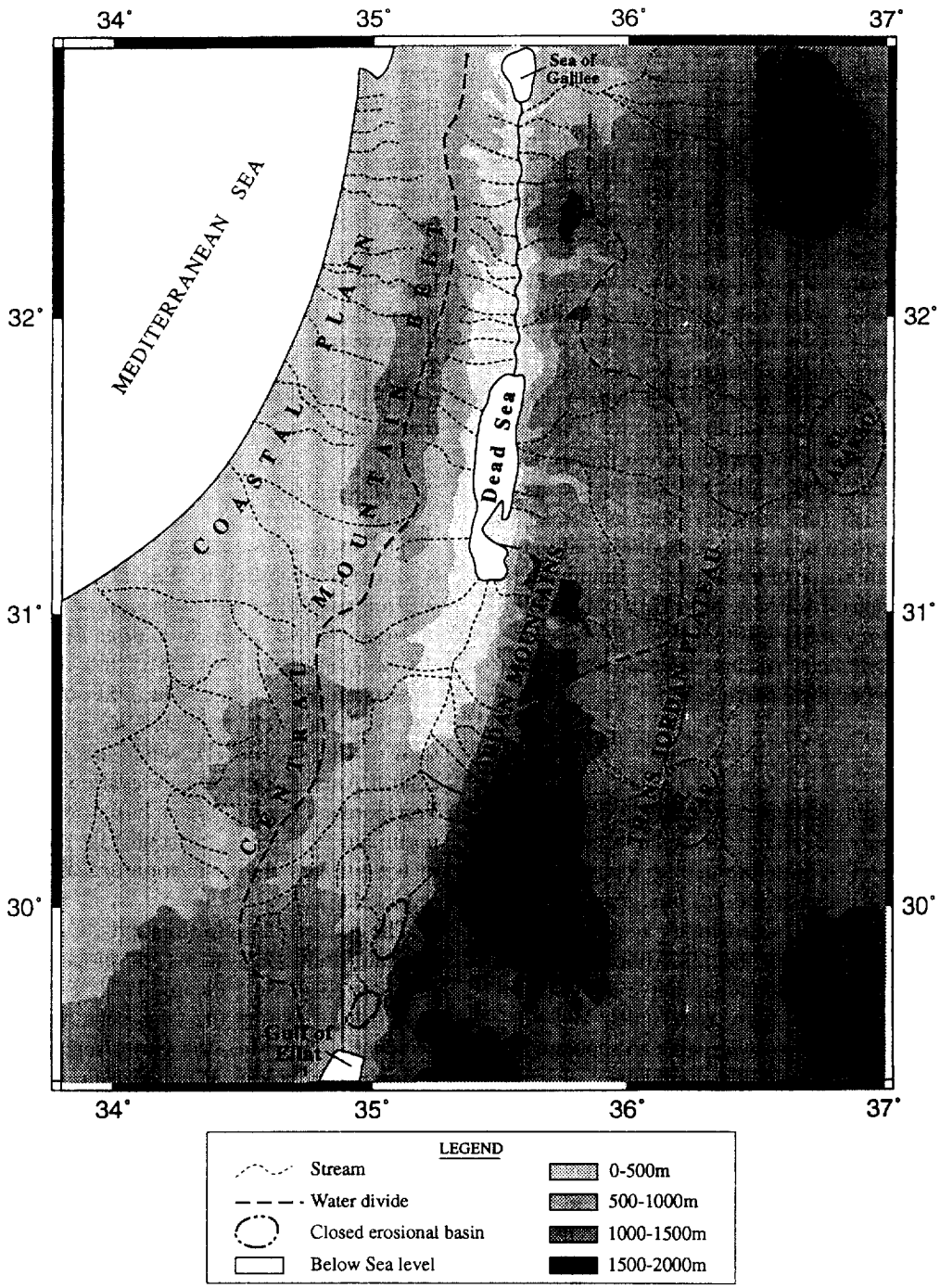


Fig. 3. Morphologic map of the studied area showing the topography (grey scale), the water divide (thick dashed lines), and the drainage networks (thin dashed lines).

basement and the Moho. The upper surface of the crystalline basement, which is detected at a depth of 3–7 km (Ginzburg and Folkman, 1981; El Isa et al., 1987; Ten Brink et al., 1990, 1993), shows an overall asymmetric pattern similar to that of the topography and structure. However, the Moho, which is detected at a depth of 20–37 km (Ginzburg and Folkman, 1980; El Isa et al., 1987; Ten Brink et al., 1990), shows an overall southeastward trend of crustal thickening that is locally thinned beneath the rift by 3–5 km. This thinning is not accompanied by significant thermal activity, as indicated by the limited volcanism within the rift and the 37.6 mW $m^{-2}$ averaged measured heat flow in the Dead Sea (Ben Avraham et al., 1978).

## 3. Model

Most quantitative investigations of asymmetric rift systems have constrained their models using three types of observations: topography, heat flow, and gravity anomalies. Large-scale geological structures, which are the best indicators of deformation, have been mostly ignored, mainly due to lack of structural data. Along the DSR, a thick sequence of sedimentary rocks provides excellent markers that allow us to trace rift-related structures over large distances across the rift. Therefore, we use the TES marker, which represent the cumulative deformation of the pre-rift topography, to constrain our model.

The model considers the sum relief of three surfaces: relief that existed prior to the formation of the rift (initial topography), relief created by slip along a curved normal boundary fault (kinematic topography), and relief created by isostatic response of the lithosphere to this faulting to additional unmodelled load (isostatic topography) (Fig. 4). We use a formulation similar to that of Weissel and Karner (1989), who considered the contribution of the two tectonic processes and additional processes, such as thermal effects, but did not include a non-zero pre-rift topography.

### 3.1. Assumptions

(1) *Northwestwardly inclined pre-rift topography.* Paleomorphological observations indicate the existence of a pre-rift regional low-relief morphology with a slight northwestward gradient. The observed southeastward inclination of the Moho suggests that the pre-rift topography was isostatically compensated.

(2) *Curved boundary fault.* Large-scale asymmetry across rift systems is often explained by displacement along an inclined or curved (listric) boundary faults (e.g., Weissel and Karner, 1989; Ebinger et al., 1991). We assume a curved boundary fault, which was found to be more appropriate to model the East African Rift (Ebinger et al., 1991).

(3) *Rigid translation along the DST.* The deformation associated with this motion is limited to the narrow rift valley and had negligible effect on the large-scale flexural structure.

(4) *Elastic behaviour of the lithosphere.* The observed large-scale flexural structure across the DSR requires a significant flexural strength of the lithosphere, which is commonly described by a flexure of an elastic plate.

(5) *Line load.* The line load approximation assumes a concentration of the load that deflects the infinitely long plate, along a line. It is justified by the narrow width of the load, which is significantly smaller than the flexural wavelength of the plate. The line load is determined from the kinematic topography (the size of the 'hole') and from an a-priori specified additional load, which represent the cumulative effect of unmodelled processes. The major unmodelled processes to affect the load are: formation of a deep sedimentary basin within the rift valley, the associated surface processes (erosion and deposition), and thermal subsidence. Because our focus is on the formation of the structural asymmetry across the DSR and not on processes that occur along the narrow rift valley, which are dominated by horizontal motion along the DST, we chose to determine a priori the line load of the unmodelled processes.

### 3.2. Formulation

Using an approach similar to that of Weissel and Karner (1989), we use two-dimensional calculations, which describe well the first-order structure along rifts, but ignore along-strike variations. Although the DSR is principally a transcurrent tectonic environment, it is still justifiable to use two-dimensional

calculations, because we assumed rigid translation along the DST.

The initial topography (Fig. 4a) is assumed to be an inclined linear surface, which is described by:

$$z_0(x) = ax + b \tag{1}$$

where $z_0$ is the initial elevation, $x$ is the distance from the rift axis, $a$ is the slope, and $b$ is the elevation of the rift axis.

The kinematic topography (Fig. 4b) develops in response to extension perpendicular to the rift axis (roughly E–W) by displacement along a curved normal boundary (listric) fault, forming an asymmetric half-graben structure. The boundary fault is assumed to be elliptical, with major axes $h$ and $d$ (Fig. 5a); $h$ is also the thickness of the upper plate. The upper plate, which is displaced horizontally by $x_0$, deforms by vertical shear to maintain contact with the lower plate (Fig. 5b). The kinematic topography is described by:

$$z_k(x) = h \times \begin{cases} 0, \text{ for } x \leftarrow (d + x_0) \\ -\sqrt{1 - \left(\dfrac{x + d + x_0}{d}\right)^2}, \\ \quad \text{for } -(d + x_0) \leq x < -d \\ -\sqrt{1 - \left(\dfrac{x + d + x_0}{d}\right)^2} + \sqrt{1 - \left(\dfrac{x + d}{d}\right)^2}, \\ \quad \text{for } -d \leq x < -x_0 \\ -\sqrt{1 - \left(\dfrac{x + d}{d}\right)^2}, \\ \quad \text{for } -x_0 \leq x < 0 \\ 0, \text{ for } x \geq 0 \end{cases}$$

The isostatic topography (Fig. 4c) develops in response to the negative mass anomaly (i.e., a hole in the crust) induced by the kinematic topography and to the additional load. The lithosphere is assumed to behave as an homogeneous elastic plate deflecting upward in response to a line load. Deflection of an elastic plate in response to a line load is described by (Turcotte and Schubert, 1982, p. 126):

$$z_i(x) = w_0 \cdot \exp\left\{-\frac{x + x_l}{\alpha}\right\} \times \left[\sin\left(\frac{x + x_l}{\alpha}\right) + \cos\left(\frac{x + x_l}{\alpha}\right)\right] \tag{3}$$

where $z_i$ is the isostatic elevation, $x_l$ is the horizontal location at which the line load is applied (centre of the negative mass), $w_0$ is the maximum amplitude of the deflection at $x = x_l$, and $\alpha$ is the flexural parameter (Turcotte and Schubert, 1982, p. 126):

$$\alpha = \left[\frac{4D}{\rho_c g}\right]^{1/4} \tag{4}$$

where $D$ is:

$$D = \frac{E t_e^3}{12(1 - \nu^2)} \tag{5}$$

$E$ is Young's modulus, $t_e$ is the elastic thickness of the lithosphere (Fig. 5), $\nu$ is Poisson's ratio, $\rho_c$ is crustal rock density, and $g$ is the acceleration due to gravity. The maximum amplitude of the deflection is:

$$w_0 = \frac{L_t \alpha^3}{8D} \tag{6}$$

where $L_t$ is the total line load equivalent to:

$$L_t = L_k + L_a \tag{7}$$

where $L_a$ is the additional load and $L_k$ is the kinematic load:

$$L_k = \rho_c g x_0 h \tag{8}$$

### 3.3. Sensitivity studies

The calculated sum topography (Fig. 6d) depends on seven free parameters (out of a total of nine parameters — Table 1): two describing the initial topography, three the kinematic topography, and two the isostatic topography. Fig. 6 shows the sensitivity of the model to these parameters. The initial slope ($a$, Eq. 1) has a minor effect on the near rift topography, but affects the topography far from the rift axis (Fig. 6a). The initial axis elevation ($b$, Eq. 1) determines the elevation of the entire region; changes

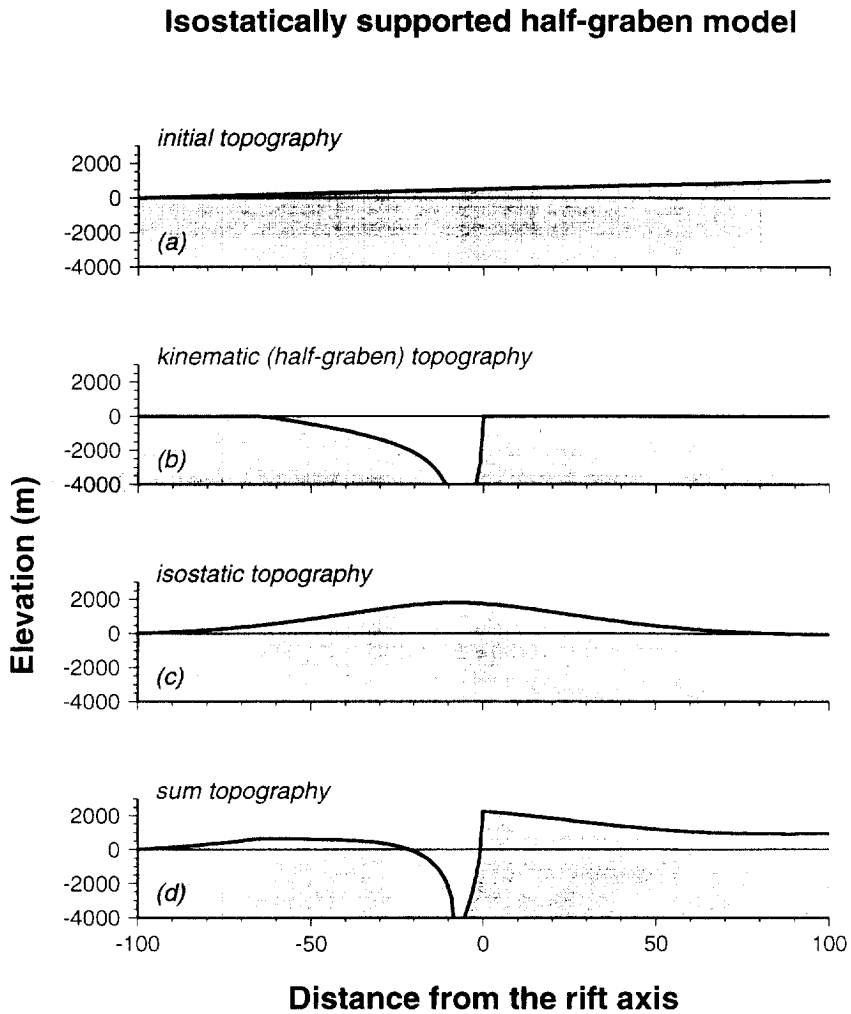


Fig. 4. An illustration of the various topography profiles calculated by the model: (a) initial topography, (b) kinematic topography, (c) isostatic topography, and (d) sum topography.

in $b$ cause a vertical translation of the topography (Fig. 6b). The fault's length ($d$, Eq. 2) determines the horizontal location of the hinge of the arch on the rift's western side (Fig. 6c). The product of the fault's height ($h$, Eq. 2) and the horizontal displacement ($x_0$, Eq. 2) determines the shape of the topography between the hinge of the arch and the rift's axis (Fig. 6d, e). The width of the upward deflecting bulge is determined by the elastic thickness ($t_e$, Eq. 5; Fig. 6f). The amplitude of the bulge is affected by several parameters: the size of the 'hole' ($x_0$ and $h$), the elastic thickness ($t_e$), and the additional load ($L_a$).

## 4. Comparison of the model's results with the observations

The model produces quantitative solutions for the large-scale structure across a rift that is formed by normal faulting and isostatic uplift. Because the model assumes an infinitely long elastic plate, it can be applied only to very wide segments along the DSR. Thus, we cannot use the five segments of Fig. 1, because they reflect topography and structure along 40–80-km-wide segments. Instead, we characterize the first-order topography and structure across the rift by calculating their average along the

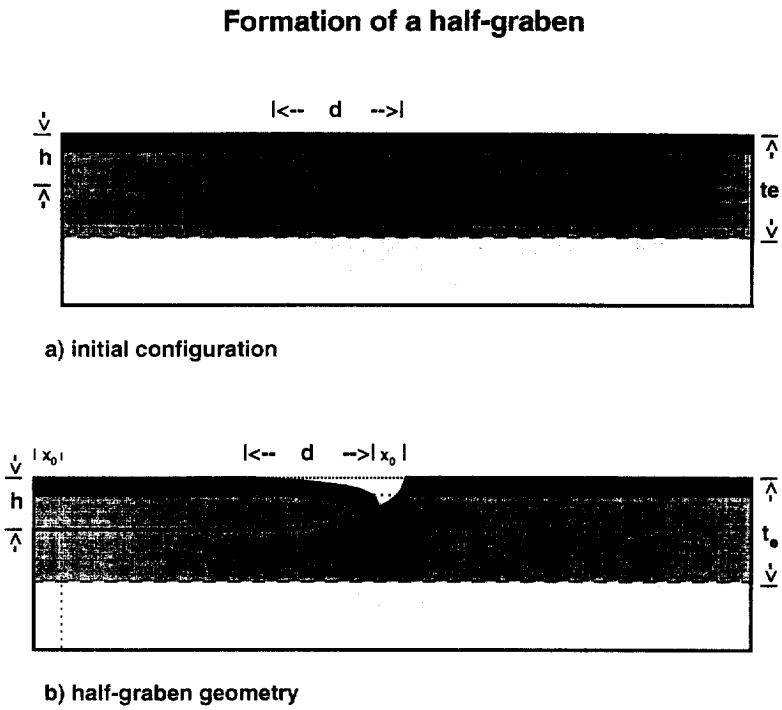


Fig. 5. Schematic illustration of the formation of a half-graben (kinematic topography): (a) initial configuration, and (b) final geometry that considers vertical shear of the upper plate to maintain contact with the lower plates. $d$ is the fault length; $h$ is the fault height; $x_0$ is the amount of horizontal displacement; and $t_e$ is the elastic thickness of the lithosphere. $d$ and $h$ are also the two major axes of the elliptical-shaped normal fault.

Table 1
Values of parameters used by the model

| Parameter | Description | Units | Segments | | |
|---|---|---|---|---|---|
| | | | 1–4 | 1–2 | 3–4 |
| $E$ | Young's modulus | GPa | 60 | 60 | 60 |
| $\nu$ | Poisson's ratio | | 0.25 | 0.25 | 0.25 |
| $\rho_c$ | Crustal density | kg m$^{-3}$ | 3000 | 3000 | 3000 |
| $a$ | Initial slope | | 0.005 | 0.0065 | 0.003 |
| $b$ | Axis elevation | km | 0.5 | 0.3 | 0.7 |
| $d$ | Fault length | km | 45 | 35 | 60 |
| $h$ | Fault height | km | 15 | 15 | 15 |
| $x_0$ | Horizontal displacement | km | 4.0 | 3.0 | 6.0 |
| $t_0$ | Elastic thickness | km | 15 | 15 | 15 |
| $L_a$ | Additional load | N m$^{-1}$ | $1.2 \times 10^{12}$ | $1.6 \times 10^{12}$ | 0 |
| $L_k$ | Kinematic load | N m$^{-1}$ | $1.8 \times 10^{12}$ | $1.35 \times 10^{12}$ | $2.7 \times 10^{12}$ |
| $L_t$ | Total load | N m$^{-1}$ | $3.0 \times 10^{12}$ | $2.95 \times 10^{12}$ | $2.7 \times 10^{12}$ |

first four segments (Fig. 7a). We exclude Segment 5, because its western side structure is not characterized by a wide arch, as predicted by the model. The average topography and structure along the 250 km length of Segments 1–4 portray the characteristic asymmetry across the DSR, but less enhanced with respect to the individual segments (Fig. 1b). Therefore, we also characterize the topography and

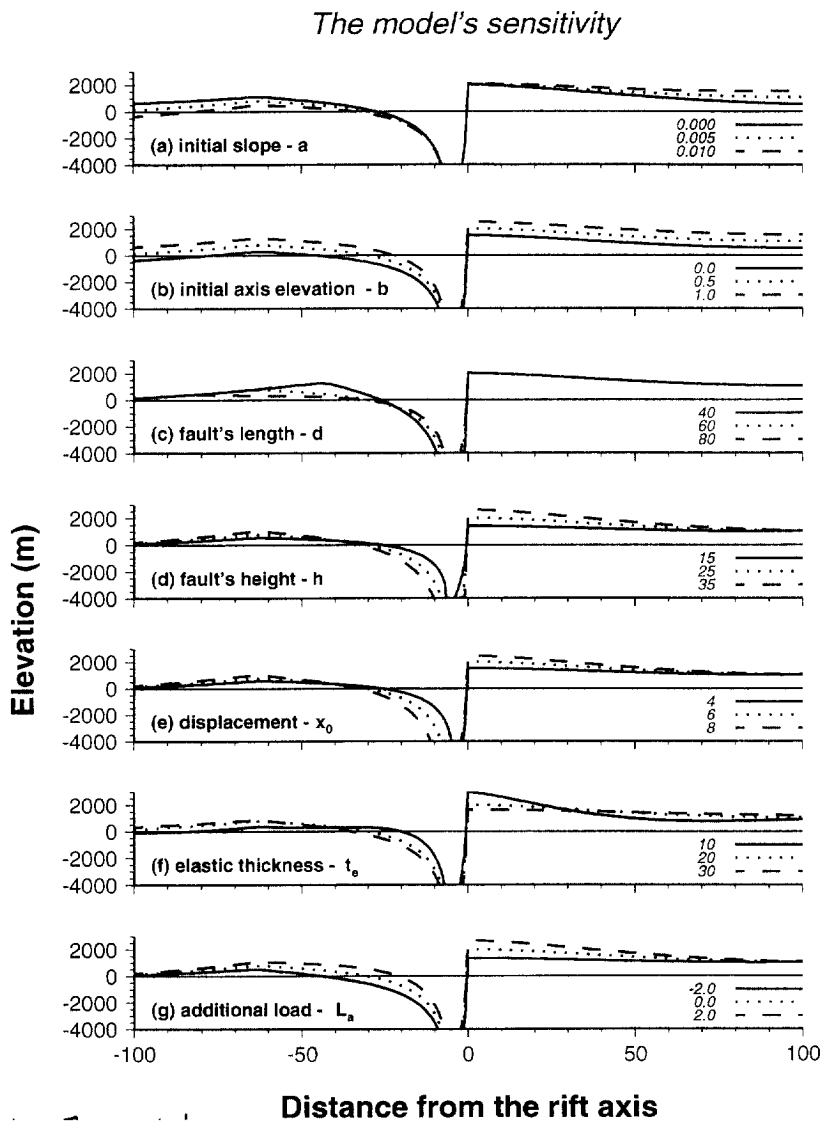


Fig. 6. Calculated topographic profiles across the rift showing the sensitivity of the model to its free parameters.

structure across the two northern and two southern segments (Fig. 7b, c), which are 120 km wide. By considering wide enough segments (>100 km), we can ignore the effect of the strike-slip motion on the observed features, because the cumulative displacement along the DST since the rift's formation is only 30 km. A rigid translation of 30 km along the DST has a minor effect on the average topography and structure of 100 km or wider segments.

The model uses six free parameters out of the total ten parameters (Table 1). This number of free parameters provides sufficient flexibility to find a combination that fits the calculated topography to the observed TES marker (Fig. 7). Because the modelled rift axis does not correspond to the morphological rift axis (the calculated axis is taken as the surface location of the boundary fault, whereas the morphological axis represents the lowest topography of the sedimentary cover that fills the rift), the calculated topography is horizontally translated by 0–6 km to the east in order to obtain a better fitting.

Fig. 7 shows a comparison between the calculated

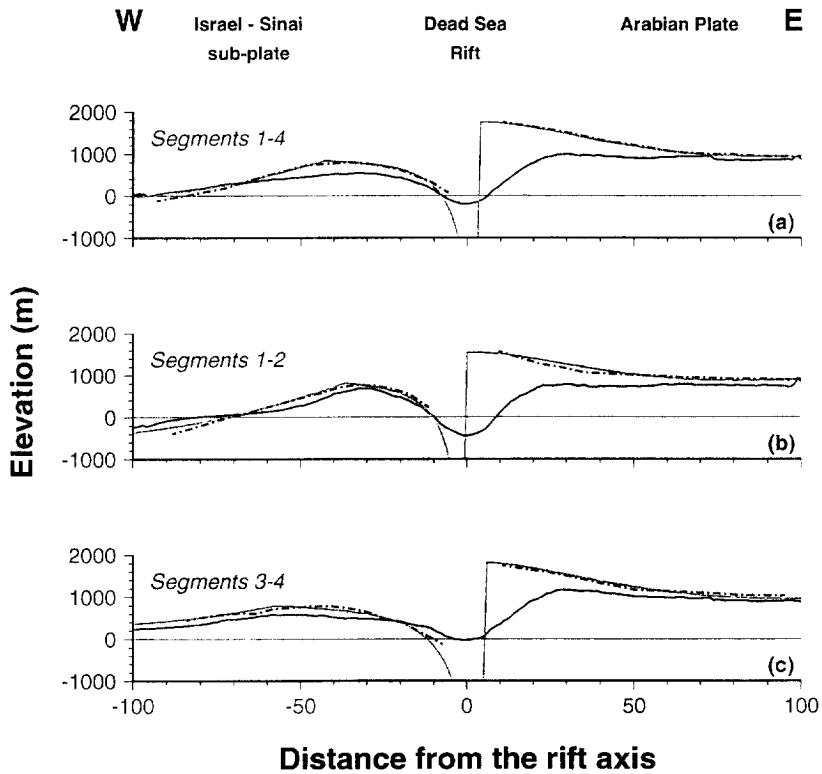


Fig. 7. A comparison between the calculated pre-rift topography (grey), and the observed TES profiles (dashed–dotted) across wide segments of the DSR. The observed topography (black) profiles are also provided for reference.

topography (grey) and the observed TES marker (dash–dotted). Good agreement between the two curves is obtained by choosing the parameter values listed in Table 1. Out of the ten parameters, we chose to fix four: Young's modulus ($E$), and Poisson's ratio ($\nu$), crustal density ($\rho_c$), and the fault's height ($h$). The fault's height is fixed at 15 km, which is roughly the depth of the brittle–ductile transition. If we choose a different value for $h$, we still obtain the same calculated topography by changing the value of the horizontal displacement ($x_0$); the same large-scale calculated topography is obtained as long as the product of these two parameters is maintained ($h \times x_0 = \text{const.}$). The other three fixed parameters determine the flexural parameter ($\alpha$, Eq. 4).

## 5. Discussion

The large-scale structural asymmetry across the DSR is successfully explained by the combined effect of two tectonic processes, normal faulting along a curved normal fault and isostatic uplift, and the consideration of a non-zero pre-rift topography. One of the compelling results of the model is its ability to quantitatively determine the horizontal displacement ($x_0$) perpendicular to the rift axis. Our results show a southward increase in the extension from 3 km in the north to 6 km in the south (Table 1). This result is consistent with the overall extension pattern along the DSR, which is very small in the north, or even compressional in Lebanon, and much higher in the south, where the rift widens and deepens along the Gulf of Elat. However, our results (Table 1) are not unique, because we fixed the fault's height ($h$) at 15 km. A better approach is to estimate $x_0$ according to a range of values for the fault's height. We estimate $h$ in the range of 10–40 km and calculate a horizontal displacement 1–4 km in the north, and 2–8 km in the south. A similar amount of extension (3–10 km) across the East African Rift was calculated by

Ebinger et al. (1991) by using a similar model. Garfunkel (1981) estimated the horizontal displacement perpendicular to the DST as 1.5–4 km, which falls on the lower end of our estimated range.

Another quantitative prediction of the model is the shape and depth of the sedimentary basin that fills the 'hole' generated by the kinematic topography. The model predicts a 4–5-km-deep prism-shaped basin that is continuous along the entire length of the rift. However, this prediction does not fit the observed trapezoid shape, nor the variable depth (1–8 km deep) of sedimentary basins along the DSR. The model fails to predicts the shape of the sedimentary basin, because it does not consider processes that occur along the narrow rift valley and are dominated by horizontal motion along the DST, such as the formation of pull-apart basins.

The model also provides quantitative estimate for the line force (total line load) that is used to calculate the upward deflection of the lithosphere in a wide area along the rift axis. Our results indicate that the isostatic uplift in the southern half of the rift can be attributed solely the kinematic load, suggesting a mass balance between the eroded rock volume from the rift margins and the deposited sediments volume within the rift valley (Fig. 7c). However, the isostatic uplift in the northern section of the studied area cannot be explained without the consideration of an additional load to that induced by the formation of the half-graben. The additional load reflects the sum effects of unmodelled processes, including thermal subsidence, surface processes, and the formation of pull-apart basin along the rift axis. The limited volcanism within the rift and the low measured heat flow in the Dead Sea (37.6 mW $m^{-2}$, Ben Avraham et al., 1978) indicate a minor thermal activity beneath the rift and a negligible contribution of thermal subsidence to the line load. Surface processes affect the line load by re-distributing the near surface rock mass. However, the short transfer of the eroded rock mass from the rift margins to the rift valley results in a minor net change of the line load, as observed along the southern half of the rift. The dominant contributor to the additional load is a negative mass anomaly of the unconsolidated sediments that fill the deep Dead Sea Basin (DSB). The DSB is a 8–10-km-deep pull-apart basin that is filled with a thick sequence of sediments that have been transported from a large drainage area (Fig. 3). The magnitude of the additional load ($1.6 \times 10^{12}$ N $m^{-1}$) is comparable to a load induced by a 20 km wide and 9 km deep basin, which is very similar to the dimensions of the DSB, that is filled with unconsolidated sediments of the density 2100 kg $m^{-3}$. Although the DSB lies along the two middle segments (Segments 2 and 3), its deepest part lies along Segment 2 (Ten Brink et al., 1993) and, therefore, its load affects the two northern segments more.

The formation of the structural arching west of the rift is also explained by the model. The arching, a wide asymmetrical fold, was formed contemporaneously with the rift and parallel to the rift axis (Picard, 1943); therefore, it cannot be explained by compression perpendicular to the fold axis (Wdowinski and Zilberman, 1996). Our model provides a mechanical explanation for its formation in a primarily extensional environment: the western slope of the arching reflects the initially inclined pre-rift topography, and the eastern slope reflects the downward flexure of the rift's western margin toward the rift axis. The wide isostatic uplift across the rift added to the arching amplitude, but did not affect its width. An alternative explanation for the arching has been discussed by Tibor et al. (1992), who proposed that the westwardly-dipping western slope of the arching reflects the subsidence of the Mediterranean coast due to the load of the Nile sediments. This mechanism was not considered in the model, because it could only be applied to the two northern segments (Segments 1 and 2), which include the Mediterranean coast (Fig. 1). In this region, it may be a viable mechanism for the steeper western slope of the arching, which was not produced by the model.

The significant change in the regional drainage system that occurred in the Early Pliocene (5 Ma) is well explained by our results. Prior to the formation of the rift, the entire region drained northwestward to the Mediterranean; this morphology is represented in the model by the initial topography (Fig. 4a). The formation of the half-graben (kinematic topography, Fig. 4b) generated two base levels (sea level in the west and rift axis in the centre) corresponding to the Mediterranean and the DSR regional drainage systems. When the isostatic topography is included (Fig. 4c), the post-rift morphology, as represented by the sum topography (Fig. 4d), shows the formation of

a third base level east of the uplifted eastern margin. This simple mechanical model for the formation of the third base level provides a good explanation for the formation of the elevated Transjordan closed drainage basins (El Azaraq and El Jafar, Fig. 3).

The mechanical properties used in the model suggest an elastic thickness of 15 km, which is less than the 20 km estimate of Ten Brink et al. (1990). Our estimate is also much less than the 40–50 km thickness obtained by Ebinger et al. (1991) for the lithosphere across the East African Rift. This difference reflects a curve fitting to a different type of observations. In this study, the model's results are compared with structural data, whereas Ten Brink et al. (1990) and Ebinger et al. (1991) fitted their results to the topography. The observed topography does not reflect the full lithospheric curvature, because erosion truncates some of the uplifted regions. However, our estimate is closer to the 4–8 km elastic thickness calculations obtained by King et al. (1988) for real structures. Our estimate of maximum deflection (1.1–1.3 km) is also different from the 0.7–0.9 km estimate of Ten Brink et al. (1990). Once again, this difference reflects the use of different type of observations.

The asymmetry observed in the central segment of the DSR is also evident across the rift's southern counterparts, the Gulf of Elat and the Red Sea. The asymmetric topography and volcanic patterns across the Red Sea were explained by Wernicke (1985) to reflect a simple shear extension of the entire lithosphere. Buck et al. (1988) quantified Wernicke's model and concluded that it cannot explain the observed topography, nor the heat flow anomalies across the Red Sea. Our model, while also based on a simple shear assumption, does succeed in fitting the observations across the DSR. The main difference between Buck et al. (1988) and the present study lies in the choice of boundary fault geometry. While Buck et al. (1988) assumed an eastward-dipping fault inclined toward the higher topography, we assume a westward-dipping boundary fault inclined toward the lower topography. We suggest that Buck's model be re-examined using an opposite geometry for the boundary fault.

The isostatically supported half-graben model is relatively simple, thus it is limited by its assumptions: it is two-dimensional, considers only the kinematic of the extension, neglects smaller-scale structures within the rift valley, and assumes a simple fault geometry and a uniform elastic behaviour of the lithosphere. Future models of such tectonic environments should consider the three-dimensional complexity of the rift geometry and the kinematics, more realistic rheology, such as visco-plastic or visco-elastic-plastic, a dynamic approach to the extension, and the effect of surface processes.

## 6. Conclusions

The major conclusions of this study are:

(1) The large-scale structure across the DSR is successfully explained by the combined effect of two tectonic processes: normal faulting along a curved boundary fault and isostatic uplift. The model predicts the observed structural asymmetry across the rift: an upward-flexed eastern margin, a downward-flexed western margin, and a wide arch west of the rift.

(2) The extension perpendicular to the rift axis lies in the range 1–4 km in the northern half of the studied area and 2–8 km in the southern half. This result is consistent with the overall extension pattern along the DSR, which is very small in the north and much larger in the south, where the rift widens and deepens along the Gulf of Elat.

(3) The isostatic uplift along the southern half of the studied area can be explained solely by the negative mass anomaly induced by the normal faulting. However, uplift along the northern half cannot be explained without the consideration of an additional load comparable in magnitude to the load induced by the kinematic topography. The additional load reflects the negative mass anomaly of the 8–10 km deep Dead Sea Basin, which is filled with unconsolidated sediments.

(4) The model also provides qualitative explanations for other observations across the rift: (a) the formation of the arching (wide fold) contemporaneously with the rift formation in a primarily extensional environment; (b) the formation of three regional drainage systems; and (c) the observed low-magnitude upward deflection of the Moho beneath the rift.

## Acknowledgements

We are thankful to H. Kooi and D. Delvaux for very helpful comments. We would also like to thank Amotz Agnon, Gidi Baer, Ariel Haiman, Ze'ev Reches, and Jilles Wust for useful discussions and comments. This study was supported by the Minerva Dead Sea Research Center at Tel Aviv University.

## References

Bell, R.B., Karner, G.D. and Steckler, M.S., 1988. Early Mesozoic rift basins of the eastern north America and their gravity anomalies: The role of detachments during extension. Tectonics, 7: 447–462.

Ben-Avraham, Z. and Zobak, M.D., 1992. Transform-normal extension and asymmetric basins: An alternative to pull-apart models. Geology, 20: 423–426.

Ben Avraham, Z., Hanel, R. and Villinger, H., 1978. Heat flow through the Dead Sea rift. Mar. Geol., 28: 253–269.

Bentor, Y. and Vroman, A., 1960. The geological map of the Negev, 1:100,000, sheet 16: Mt. Sedom, with explanatory text (revised ed.). Israel Geological Survey. Jerusalem, 117 pp.

Buck, W.R., Martinez, M., Steckler, M.S. and Cochran, J.R., 1988. Thermal consequences of lithospheric extension: pure and simple. Tectonics, 7: 213–234.

Ebinger, C.J., Bechtel, T.D., Forsyth, D.W. and Bowin, C.O., 1989. Effective elastic plate thickness beneath the East African and Afar Plateaus and dynamic compensation of the uplift. J. Geophys. Res., 94: 2883–2901.

Ebinger, C.J., Karner, G.D. and Weissel, J.K., 1991. Mechanical strength of extended continental lithosphere: constraints from the western rift system, East Africa. Tectonics, 10: 1239–1256.

El Isa, Z., Mechie, J., Prodehl, C., Makris, J. and Rihmn, R., 1987. A crustal structure study of Jordan derived from seismic refraction data. Tectonophysics, 138: 235–253.

Freund, R., Garfunkel, Z., Zak, I., Goldberg, M., Weissbrod, T. and Derin, B., 1970. The shear along the Dead Sea Rift. Philos. Trans. R. Soc. London, Ser. A, 267: 107–130.

Garfunkel, Z., 1981. Internal structure of the Dead Sea leaky transform (rift) in relation to plate kinematics. Tectonophysics, 80: 81–108.

Garfunkel, Z. and Horowitz, A., 1966. The upper Tertiary and the Quaternary morphology of the Negev. Isr. J. Earth Sci., 15: 101–117.

Ginzburg, A. and Folkman, Y., 1980. The crustal structure between the Dead Sea Rift and the Mediterranean Sea. Earth Planet. Sci. Lett., 51(1): 181–188.

Ginzburg, A. and Folkman, Y., 1981. Geophysical investigation of crystalline basement between Dead Sea Rift and Mediterranean Sea. Am. Assoc. Pet. Geol. Bull., 65: 490–500.

Joffe, S. and Garfunkel, Z., 1987. Plate kinematics of the circum Red Sea — a re-evaluation. Tectonophysics, 141: 5–22.

King, G.C.P., Stein, R.S. and Rundle, J.B., 1988. The growth of geological structures by repeated earthquakes, 1. Conceptual framework. J. Geophys. Res., 93: 13,307–13,318.

Picard, L., 1943. Structure and evolution of Palestine. Geol. Dep. Hebrew Univ., Jerusalem, Bull., 187 pp.

Picard, L., 1951. Geomorphogeny of Israel, 1. The Negev. Isr. Geol. Surv. Bull., 1: 1–28 (Reprint from Isr. Res. Counc. Bull., 1951, 1–2: 5–32).

Picard, L., 1966. Thoughts on the graben systems of the Near East. Geol. Surv. Can., Pap., 66-14: 22–34.

Picard, L., 1987. The Elat (Aqaba)–Dead Sea–Jordan subgraben system. Tectonophysics, 141: 23–32.

Quenell, A.M., 1959. Tectonics of the Dead Sea Rift. 20th Int. Geol. Congr., Mexico, pp. 385–405.

Rosendahl, B.R., 1987. Architecture of continental rift with special reference to East Africa. Annu. Rev. Earth Planet. Sci., 15: 445–503.

Ten Brink, U.S., Schoenberg, N., Kovach, R.L. and Ben-Avraham, Z., 1990. Uplift and possible Moho offset across the Dead Sea transform. In: R.L. Kovach and Z. Ben-Avraham (Editors), Geologic and Tectonic Processes of the Dead Sea Rift Zone. Tectonophysics, 180: 71–85.

Ten Brink, U., Ben Avraham, Z., Bell, R.E., Hassouneh, M., Coleman, D.F., Andreasen, G., Tibor, G. and Coakley, B., 1993. Structure of the Dead Sea pull-apart basin from gravity analyses. J. Geophys. Res., 98: 21,877–21,894.

Tibor, G., Ben-Avraham, Z., Steckler, M. and Fligelman, H., 1992. Late Tertiary subsidence history of the Southern Levant Margin, Eastern Mediterranean Sea, and its implications to the understanding of the Messinian event. J. Geophys. Res., 97: 17,593–17,614.

Turcotte, D.L. and Schubert, G., 1982. Geodynamics, Application of Continuum Physics to Geological Problems. Wiley, New York, NY, 450 pp.

Wdowinski, S. and Zilberman, E., 1996. Systematic analyses of the large scale topography and structure across the Dead Sea Rift. Submitted to Tectonics.

Weissel, J.K. and Karner, G.D., 1989. Flexural uplift of rift flanks due to mechanical unloading of the lithosphere during extension. J. Geophys. Res., 94: 13,919–13,950.

Wernicke, B., 1985. Uniform-sense normal simple shear of the continental lithosphere. Can. J. Earth Sci., 22: 108–125.

Wilson, J.T., 1965. A new class of faults and their bearing on continental drift. Nature, 2071: 343–347.

Zilberman, E., 1984. The Tertiary and the Quaternary of the northwestern Negev. In: Z.B. Begin (Editor), Outlines of the Geology of the Northwestern Negev. Isr. Geol. Surv. Rep. GSI/19/84: 41–76.

Zilberman, E., 1992. Remnants of Miocene landscape in the central and northern Negev and their paleogeographic implications. Isr. Geol. Surv. Bull., 83: 1–54.